

Mathematical Modeling and Experimental Studies of Twin-Screw Extrusion of Filled Polymers

DILHAN M. KALYON, ADENIYI LAWAL, RAHMI YAZICI,
PIRAYE YARAS, and SUDHIR RAILKAR

*Highly Filled Materials Institute
Stevens Institute of Technology
Castle Point on the Hudson
Hoboken, New Jersey 07030*

Extrusion of filled polymers is commonly employed in diverse industries including compounding operations. The analysis of extrusion of filled polymers is complicated especially by the ubiquitous viscoplasticity and wall slip of the filled polymers. Furthermore, the role played by entrainment of air in the processor, the continuously evolving microstructure, and hence the rheological behavior of the filled polymer in the mixing volume of the extruder and the flow instabilities associated with the converging flows involving the filtration of the binder polymer present additional challenges to the analysis. Specialized techniques are also necessary to quantitatively describe the dispersive and the distributive degree of mixing of the compound. The principal tasks of this study included the collection of experimental data from twin-screw extrusion using an instrumented and industrial-scale co-rotating extruder in conjunction with a well-characterized filled polymer, which exhibits viscoplasticity and wall slip. The process allowed the adequate mixing of the ingredients and the removal of its air content. Next, the processing data were compared with the results of numerical simulation using the Finite Element Method. The predictions compared favorably with the experimental temperature and pressure distributions obtained under different sets of operating conditions. The distributive degree of mixing (spatial homogeneity) of the filled polymer upon exit from the die was also characterized employing a wide angle X-ray diffraction technique in spite of the amorphous nature of both the filler and the binder polymer, i.e., hollow glass spheres and poly(dimethyl siloxane) polymer.

INTRODUCTION

The study focuses on the extrusion of filled polymers in the widely used fully intermeshing co-rotating twin-screw extruder. Twin-screw extruders are used for a variety of industrial tasks including melting, pressurization, mixing, blending, compounding, and reactive extrusion (1–3). Various mathematical models of the co-rotating twin-screw extrusion at differing degrees of complexity were reported (4–22). Experimental investigations were also carried-out to elucidate the flow mechanism occurring in co-rotating twin-screw extruders (23–32).

Among many applications of twin-screw extruders, the compounding of filled polymers deserves special attention. The continuous processing of such filled systems is affected by the generally observed viscoplasticity (33) and the concomitant wall slip behavior (34–38). Special rheological methods are necessary for the characterization of the wall slip behavior of con-

centrated suspensions (34–37). Previous studies have demonstrated that the wall slip plays an important role in determining the extrudability of filled polymers (39–47). However, simulation studies of flow behavior of concentrated suspensions, and comparison of these simulations with experimental data collected from industrial scale extruders are lacking.

Here, we present the results of a comprehensive study that combines detailed material characterization, experimental studies using a well-instrumented twin-screw extruder, mathematical modeling of the co-rotating twin-screw extrusion to analyze the processability behavior of filled polymers and specialized X-ray techniques to characterize the distributive degree of mixing of the filler in the polymer. Specifically, the study was focused on the pressurization and concomitant heat transfer occurring in the regular flighted screw sections of the co-rotating twin-screw extruder following adequate mixing and deaeration of the sus-

pension. The evolving nature of the microstructure and hence the rheological behavior of the suspension as the mixing progresses in the mixing volume of the processor and the role played by air will also be discussed. It should be noted that the experimental techniques and the simulation methods described here are equally valid for other types of single and twin-screw extruders.

NUMERICAL ANALYSIS

Geometry

Two-tipped self-wiping screw elements for which the flight width is relatively small compared with the channel width were used (Fig. 1). Under such circumstances, the flow channels can be assumed to be continuous from one screw element to the other, without a change in size, similar to that in a single screw extruder. Although three dimensional FEM based methods capable of describing the geometry without unwrapping are available (14, 18) the use of a continuous channel without curvature is sufficiently realistic (9) and provides significant savings in computation time.

Flow Equations

The flow in the channel is governed by the general equations of the conservation of mass and momentum, which are elliptic and three-dimensional, but the solution of the complete set of equations is unwarranted. The flow is assumed to be steady. The inertia effects are neglected for the generally highly viscous nature of the polymers and suspensions utilized in extrusion and the creeping nature of the resulting flow. Furthermore, the velocity derivatives along the channel are small in comparison with those in the transverse directions, except at locations close to the entrance of the channel. With these considerations, the governing equations are parabolic, and, therefore, a step-wise integration in the z direction (primary flow direction indicated in Fig. 1) at prescribed upstream conditions can be carried out. The equations of conservation of mass and momentum become:

$$\frac{\partial u_x}{\partial x} + \frac{\partial u_y}{\partial y} + \frac{\partial u_z}{\partial z} = 0 \tag{1}$$

$$\frac{\partial \bar{p}}{\partial x} = \frac{\partial}{\partial x} \left(2\eta \frac{\partial u_x}{\partial x} \right) + \frac{\partial}{\partial y} \left\{ \eta \left(\frac{\partial u_x}{\partial y} + \frac{\partial u_y}{\partial x} \right) \right\} \tag{2a}$$

$$\frac{\partial \bar{p}}{\partial y} = \frac{\partial}{\partial y} \left(2\eta \frac{\partial u_y}{\partial y} \right) + \frac{\partial}{\partial x} \left\{ \eta \left(\frac{\partial u_x}{\partial y} + \frac{\partial u_y}{\partial x} \right) \right\} \tag{2b}$$

$$\frac{dp_m}{dz} = \frac{\partial}{\partial x} \left(\eta \frac{\partial u_z}{\partial x} \right) + \frac{\partial}{\partial y} \left(\eta \frac{\partial u_z}{\partial y} \right) \tag{2c}$$

The parabolic nature of these differential equations is preserved through p_m , the mean viscous pressure that has been defined for the primary flow direction, z, and

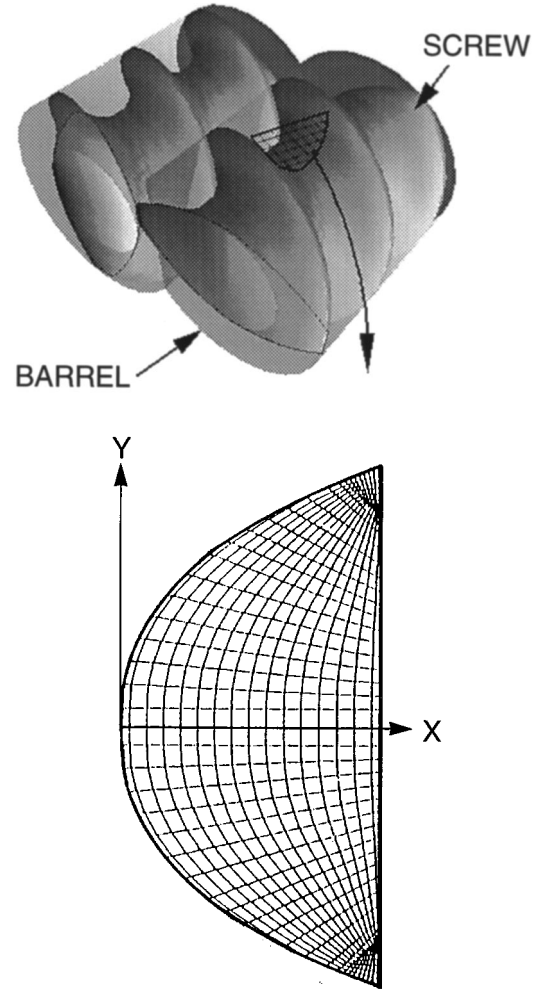


Fig. 1. Fully flighted screw section of the co-rotating twin-screw extruder.

is constant for any x-y plane. The downchannel direction pressure gradient, dp_m/dz , which is a function of the channel direction coordinate, z, for temperature dependent shear viscosity, is determined by the requirement that the conservation of mass constraint on the total volumetric flow rate, Q, is satisfied:

$$Q - \int_D u_z dD = 0 \tag{3}$$

where Q is set by the specified inlet value of dp_m/dz and D is the cross-sectional area available for flow. The pressure, \bar{p} , is allowed to vary in the transverse directions in such a way that the continuity equation (Eq 1) is satisfied (44). Even though u_z varies along the downchannel direction, z, it is assumed in Eq 1 that step sizes in z direction are sufficiently small so that $\partial u_z/\partial z$ is negligible compared to the other two terms. Equations 2a-b can now be handled separately from the channel direction Equation 2c and the penalty method is used in approximating the pressure, \bar{p} .

Boundary Conditions and Implementation of Wall Slip

Applying Bubnov-Galerkin's method to Eqs 2a-b leads to the following dimensionless residual equations (44):

$$\int_D \nabla \pi \cdot \underline{\mathbf{T}} dD - \int_{\Gamma_s} \pi (\mathbf{n} \cdot \underline{\mathbf{T}}) d\Gamma_s = \mathbf{0} \quad (4)$$

where π is the weighting function and $\underline{\mathbf{T}}$ is the total stress tensor. On the boundaries, Γ_s , the traction $\mathbf{n} \cdot \underline{\mathbf{T}}$ can be decomposed into the tangential and normal components to obtain:

$$\int_D \nabla \pi \cdot \underline{\mathbf{T}} dD - \int_{\Gamma_s} \pi (\mathbf{nt}:\underline{\mathbf{T}}) \mathbf{t} d\Gamma_s - \int_{\Gamma_s} \pi (\mathbf{nn}:\underline{\mathbf{T}}) \mathbf{n} d\Gamma_s = 0 \quad (5)$$

where \mathbf{t} and \mathbf{n} are, respectively, the unit tangent and the unit outward normal vectors to the solid boundary. The conditions of wall slip and no material exchange between the fluid and the boundary in dimensionless form can be expressed as:

$$\mathbf{t} \cdot (\mathbf{u} - \mathbf{u}_{solid}) = \beta^* (\mathbf{nt}:\underline{\mathbf{T}}) \quad (6)$$

$$\mathbf{n} \cdot (\mathbf{u} - \mathbf{u}_{solid}) = 0 \quad (7)$$

where \mathbf{u}_{solid} is the solid boundary velocity vector, \mathbf{u} is the fluid velocity vector and $\beta^* = (m_0 \omega^{n-1} / R_s) \beta$ is the dimensionless Navier's slip coefficient and $\beta = 0$ gives no slip. Equation 6 is the Navier's slip condition as applicable to the two-dimensional transverse plane (48).

The essential condition of normal velocity is transformed into a natural condition (49):

$$\mathbf{nt}:\underline{\mathbf{T}} = \frac{\mathbf{t} \cdot (\mathbf{u} - \mathbf{u}_{solid})}{\beta^*} \quad (8a)$$

$$\mathbf{nn}:\underline{\mathbf{T}} = \frac{\mathbf{n} \cdot (\mathbf{u} - \mathbf{u}_{solid})}{\lambda_s} \quad (8b)$$

where a new penalty parameter, λ_s , has been introduced. As $\lambda_s \rightarrow 0$, Eq 8b becomes equivalent to Eq 7 since the normal component of the traction must be finite at the boundary. In practice, a λ_s value in the range $10^{-10} - 10^{-18}$ produces a normal velocity difference of the same order of magnitude. Equations 8a-b are now substituted into Eq 5 to give:

$$\int_D \nabla \pi \cdot \underline{\mathbf{T}} dD - \int_{\Gamma_s} \pi \frac{\mathbf{t} \cdot (\mathbf{u} - \mathbf{u}_{solid})}{\beta^*} \mathbf{t} d\Gamma_s - \int_{\Gamma_s} \pi \frac{\mathbf{n} \cdot (\mathbf{u} - \mathbf{u}_{solid})}{\lambda_s} \mathbf{n} d\Gamma_s = \mathbf{0} \quad (9)$$

For the channel direction momentum equation, the normal component of traction does not exist and this makes the incorporation of wall slip by the Galerkin method straightforward. The components of \mathbf{u}_{solid} on the screw root surface are all zero, while on the barrel, the solid boundary velocity \mathbf{u}_{solid} , is given in dimensionless form as:

$$\mathbf{u}_{solid} = \mathbf{i} \sin \phi_h + \mathbf{k} \cos \phi_h \quad (10)$$

where ϕ_h is the helix angle of the screw and, \mathbf{i} and \mathbf{k} are unit vectors in x- and z-directions, respectively.

Viscoplasticity

The filled polymer is assumed to be a purely viscous fluid, the rheological behavior of which is described by the generalized Newtonian fluid constitutive relation:

$$\underline{\boldsymbol{\tau}} = - \eta(\dot{\gamma}) \dot{\underline{\boldsymbol{\gamma}}} \quad (11)$$

where η is the shear viscosity material function, $\dot{\underline{\boldsymbol{\gamma}}}$ is the rate-of-deformation tensor and $\dot{\gamma}$ is the second invariant of the rate of deformation tensor. The dependence of the shear viscosity material function on the deformation rate and temperature follows the modified Herschel-Bulkley model (50):

$$\eta = \left(m_0 |\dot{\gamma}|^{n-1} + \frac{\tau_y (1 - \exp(-n_b |\dot{\gamma}|))}{|\dot{\gamma}|} \right) \exp(-c'(T - T_0)) \quad (12)$$

where n is a material parameter which governs the sensitivity of the fluid to deformation rate, τ_y is the apparent yield stress, n_b is the stress growth exponent, c' is the temperature coefficient of viscosity, T_0 is the entrance temperature used as the reference temperature. The magnitude of the rate-of-deformation tensor $|\dot{\gamma}|$ is defined for our case, by:

$$|\dot{\gamma}|^2 = 2u_{x,x}^2 + 2u_{y,y}^2 + (u_{x,y} + u_{y,x})^2 + u_{z,x}^2 + u_{z,y}^2 \quad (13)$$

where the comma indicates differentiation. If we introduce the following dimensionless variables:

$$|\dot{\gamma}| = \omega |\dot{\gamma}|^*, \tau_y = m_0 \omega^n \tau_y^*, n_b = n_b^* / \omega \quad (14)$$

then Eq 12, in dimensionless form, becomes:

$$\eta^* = \left((|\dot{\gamma}|^*)^{n-1} + \frac{\tau_y^* (1 - \exp(-n_b^* |\dot{\gamma}|^*))}{|\dot{\gamma}|^*} \right) \exp(-c'(T - T_0)) \quad (15)$$

Various methods of determining the yield behavior of viscoplastic materials were recently used and compared (38).

Energy Equation and Boundary Conditions

Polymer melts generally have low thermal conductivity and moderately high values of ρ and C_p , and hence exhibit high Péclet numbers. It has been demonstrated by Lawal and Kalyon (44), that the transverse convection terms are generally not negligible when compared with either the downchannel convection term or the transverse heat conduction terms. On the other hand, except for low mass flow rates (hence low Péclet numbers), and the region close to the entrance, the heat conduction term in the down channel direction can be ignored. The fluid enters the screw channel at a temperature T_0 . The barrel temperature is designated as T_b . Assuming steady state

conditions, and using the dimensionless temperature $\theta = (T - T_0)/(T_b - T_0)$, the energy equation in dimensionless form becomes:

$$Pe \left(u_x \frac{\partial \theta}{\partial x} + u_y \frac{\partial \theta}{\partial y} + u_z \frac{\partial \theta}{\partial z} \right) = \left(\frac{\partial^2 \theta}{\partial x^2} + \frac{\partial^2 \theta}{\partial y^2} \right) + G\eta^* (|\dot{\gamma}|^*)^2 \quad (16)$$

where $G = m_0 \omega^{n-1} (\omega R_s)^2 / k(T_b - T_0)$ is the Griffith number that indicates the relative importance of viscous dissipation effects in comparison to heat conduction.

The boundary conditions were constant barrel temperature (determined in the experimental studies) and adiabatic screw surface. In dimensionless form, the initial and boundary conditions become:

$$\text{at } z = 0 \quad \theta = 0 \quad (17a)$$

on the barrel surface

$$\theta = 1 \quad (17b)$$

on the screw surface,

$$\partial \theta / \partial \mathbf{n} = \mathbf{0} \quad (17c)$$

where \mathbf{n} is the unit vector normal to screw surface. Since the velocity distribution can be determined, this parabolic problem can be solved in a stepwise fashion along the channel direction z . The recently developed SUPG method was used in the analysis of the twin-screw extrusion (51–53). This method has been successfully implemented for single screw extrusion by Lawal and Kalyon (44) by introducing weighting functions of the form:

$$\bar{W}^f = W^f + w^f \quad (18)$$

where W^f is a continuous function of space and w^f is a discontinuous perturbation of W^f . The weighted residual form of the energy equation is then given by:

$$\int_z^{z+\Delta z} \left\{ \int_D \left[\bar{W}^f Pe \left(u_x \frac{\partial \theta}{\partial x} + u_y \frac{\partial \theta}{\partial y} + u_z \frac{\partial \theta}{\partial z} \right) + \nabla \bar{W}^f \cdot \nabla \theta - \bar{W}^f G (|\dot{\gamma}|^*)^2 \eta^* \right] dD - \int_{\Gamma_s} \bar{W}^f (\nabla \theta \cdot \mathbf{n}) d\Gamma_s \right\} dz = 0 \quad (19)$$

Following Hughes *et al.*, the perturbation function is taken as dependent on the flow field and an element mesh parameter (54). The coupled set of conservation equations, the constitutive equation and the wall slip boundary condition were solved for a broad range of operating conditions. However, the relatively low flow rate region presented additional challenges as described below.

Low Volumetric Flow Rate

During extrusion the flow in the downchannel direction is a combination of drag and pressure flows. For pure drag flow, the downchannel velocity, U_z^* , of the fluid increases monotonically from the screw root

to the maximum value at the moving barrel. However, as the value of the positive pressure gradient increases from zero, a back flow in the z^* direction appears adjacent to the screw root. The strength of this pressurization-induced back flow and the size of the back flow region depend on the operating conditions, including the positive pressure gradient, as well as the shear viscosity material function of the fluid. For the condition of positive z -velocity everywhere in the channel, i.e., $U_z^* > 0$, the downchannel convection term in the energy equation renders it suitably parabolic for stepwise integration in the downchannel direction from upstream conditions. However, when back flow occurs in some region of the channel (i.e., $U_z^* < 0$), the energy equation is no longer parabolic, but elliptic, i.e., the temperature profile at each downchannel location is affected by both upstream and downstream conditions. The volume flow rate, at which the transition from parabolic to elliptic energy equation takes place, generally depends on the operating conditions and the shear viscosity.

As the volumetric flow rate decreases the pressure gradient increases and hence the back flow, i.e., negative velocity zone becomes more pronounced. Thus, at sufficiently low volumetric flow rates the inclusion of the downchannel heat conduction term in the energy equation may be necessary. Therefore, Eq 16, which is parabolic in the z direction, needs to be replaced by the elliptic equation:

$$Pe \left(u_x \frac{\partial \theta}{\partial x} + u_y \frac{\partial \theta}{\partial y} + u_z \frac{\partial \theta}{\partial z} \right) = \left(\frac{\partial^2 \theta}{\partial x^2} + \frac{\partial^2 \theta}{\partial y^2} + \frac{\partial^2 \theta}{\partial z^2} \right) + G\eta^* (|\dot{\gamma}|^*)^2 \quad (20)$$

The presence of the second derivative of temperature in the downchannel direction in Eq 20 requires the specification of temperature or flux boundary condition not only at the entrance to the filled pressurization section of the extruder but also at the extruder exit plane located prior to entering the die. This poses a numerical difficulty as neither the temperature nor the flux distribution is known at the exit of the extruder section. A more realistic representation of the flow and heat transfer near the end of the pressurized region will require a fully three-dimensional analysis of the twin-screw extruder and the die with the rotating screw tips incorporated in the analysis. This is the approach adopted by Lawal, *et al.* (55). The Streamline Upwind/Petrov Galerkin (SUPG) technique used here in the solution of the equation of energy has the capability to suppress the instabilities generated by the change in sign of the z -velocity within the transverse to flow direction domain. However, if the volumetric flow rate decreases below a critical value, the suppression capability of SUPG breaks down and the solution becomes unstable.

One remedy is to replace the downchannel velocity U_z^* by the velocity along the axial direction of the extruder and modify the convection term appropriately

(56). However, this formulation is inconsistent since the convection and conduction terms are referred to in different coordinate systems and the method is not applicable when the curvature of the screw profile is included. Our solution is based on the determination that for high volume flow rates the SUPG technique with a suitably selected upwind parameter value produces oscillation free and smooth temperature profiles. To obtain the solution for the relatively small flow rates used in the experiments a procedure detailed elsewhere (47) was used. In this calculation procedure, the flow rate is gradually decreased and the bulk temperature variation with volume flow rate at selected downchannel locations is obtained. The bulk temperature at the desired low volume flow rate is obtained by extrapolation from the simulation runs carried-out at higher flow rates at which SUPG is sufficiently robust to suppress the oscillations. The calculations at the lower flow rates are then made under isothermal conditions, but utilizing the shear viscosity at the correct bulk temperature of the fluid as obtained with the extrapolation procedure.

EXPERIMENTAL

Materials

The polymer was poly(dimethyl-siloxane) available from Dow Corning as Silicone (200) and the filler was soda-lime borosilicate hollow glass spheres available from Potters Industries Inc., as Spherical (CAS# 65997-17-3). The solid loading level was 60 vol%. The densities of silicone 200 and hollow glass spheres approached neutral buoyancy. Their values were 980 kg/m³ and 1098 kg/m³, respectively. The thermal conductivity, k , of the suspension was 0.206 W/(m °C) and its specific heat capacity, C_p , was 1078 J/(kg°C). The twin-screw extrusion was carried-out under conditions in which the filler did not undergo attrition.

Twin-Screw Extrusion Experiments

A Baker Perkins Inc. twin-screw extruder (MP 50) with a length-to-diameter ratio of 15 was employed. The extruder was equipped with six pressure trans-

ducers, thermocouples and an adjustable-gap slit rheometer equipped with its own pressure transducers (57). The screw configuration is shown in Fig. 2. The mixing section (A-D) is followed by a devolatilization section (E), which consists of 12.7 mm pitch single elements with a total axial length of 152.4 mm followed by four kneading disks 12.7 mm wide staggered at 60° reverse. The last section is the pressurization section (G) and consisted of 279.4 mm axial length of double channel elements with a 50.8 mm lead. This section was deliberately left rather long so that at least four pressure transducers could be installed. The analysis and experiments thus focused on the flow and heat transfer of the well-mixed and devolatilized suspension occurring in this zone (G), which precedes the die flow.

A computerized data acquisition system was used to collect the processing information. The data principally included pressure distributions in the pressurization section of the extruder adjacent to the die. Temperatures at two locations were also collected. The experiments systematically varied the mass flow rate, screw speed and barrel temperature profile. The shear viscosity of the suspension could also be characterized by the adjustable gap on-line slit rheometer used as the die of the extrusion system (57).

Rheological Characterization of the Concentrated Suspension

The filled polymer, mixed and processed in the twin-screw extruder, was characterized using the slit on-line rheometer of the extruder, capillary flow, and steady torsional flow. The capillary experiments were carried out by employing an Instron Universal Tester equipped with an Instron Capillary Rheometer. Parallel disk fixtures with a 25 mm radius were used in conjunction with a Rheometrics System IV for steady torsional flow (58). A tracer technique was also used to determine the residence time and velocity distribution of the filled polymer in capillary flow (58).

Typical apparent shear stress versus shear rate data for the filled polymer collected with a series of capillar-

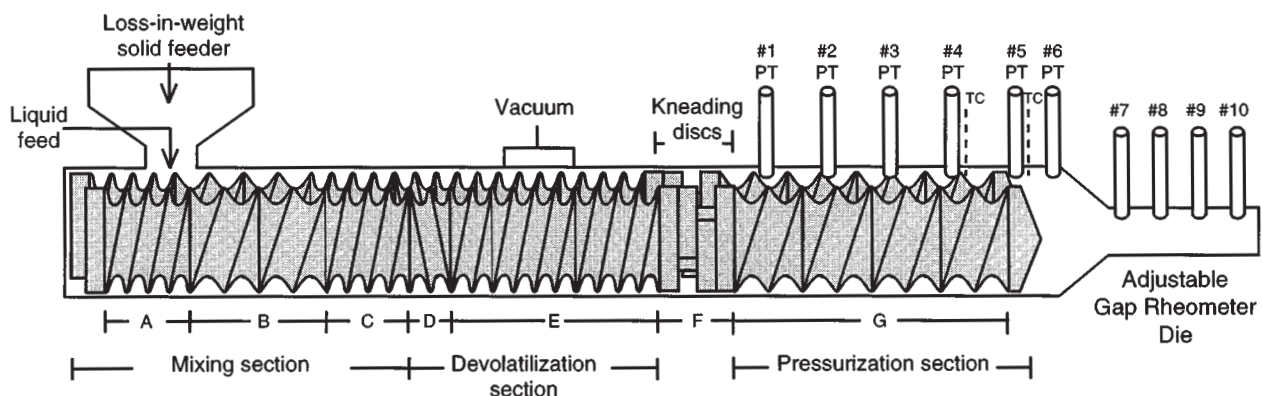
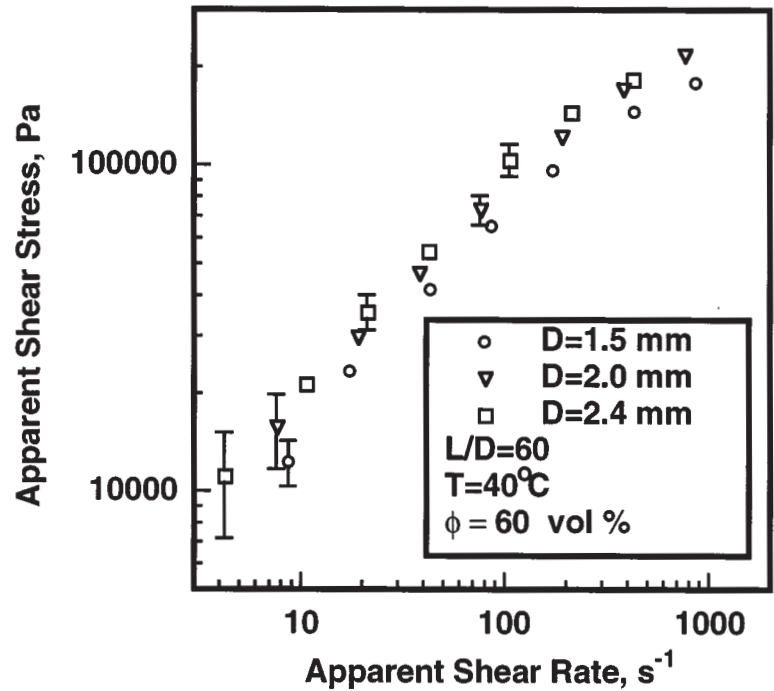


Fig. 2. Screw configuration of the twin-screw extruder used in this study.

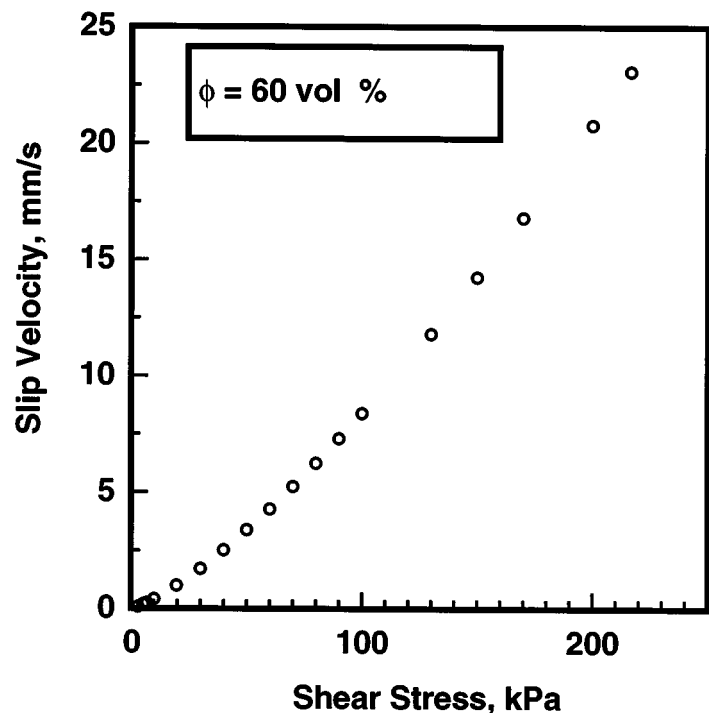
Fig. 3. Typical apparent shear stress versus apparent shear rate data for the 60 vol% suspension.



ies are shown in Fig. 3. The length/diameter, L/D ratio for all of the capillaries was 60 but the diameters changed. The wall shear stress values were corrected for the entrance and exit effects using Bagley correction. The shear stress values increase with increasing capillary diameter at a constant apparent shear rate indicating the presence of wall slip. The slip velocity

versus shear stress behavior of the suspension is shown in Fig. 4 (58). The slip velocity was assumed to vary linearly with wall shear stress and the Navier's slip coefficient, β , is equal to 9.6×10^{-5} mm/(Pa·s). The best fit of data to the Herschel-Bulkley constitutive equation gave an apparent yield stress value of 20 Pa, consistency index, m , of 6888 Pa·s^{0.43} and the ex-

Fig. 4. Slip velocity vs. shear stress behavior of the 60 vol% concentrated suspension.



ponent n was determined as 0.43. The temperature coefficient of viscosity, c' , of the suspension was characterized as 0.00395/K.

Degree of Mixing of the Concentrated Suspension

Yazici and Kalyon (59–62) have developed and applied electron probe and X-ray diffraction techniques to the analysis of degree of mixing in various filled polymers. In the present work, the wide angle X-ray diffraction method (59–62) was used. The experimental WAXD patterns from the silicone oil and the glass beads used are shown in Fig. 5. Although both materials primarily consist of Si-O molecules, and both are amorphous, because of their microstructural characteristics they exhibit unique diffraction patterns. The silicone oil exhibits a strong amorphous peak at the Bragg angle, 2θ , of 12° . This corresponds to a short-range order inter-molecular spacing of 0.74 nm. The tail observed at higher angles in this pattern emanates from the short-order regularity of molecules at smaller spacings. The diffraction pattern of the glass beads on the other hand exhibits an amorphous peak at $2\theta = 24.5^\circ$ that corresponds to a 0.36 nm average spacing of (Si, Ca, K, Al, Na)-O molecules.

The two diffraction patterns overlap in the 2θ space, as shown in Fig. 5, where they have been superposed. Analysis of such a diffraction pattern for identification of the components present and the quantitative determination of their concentration in the mixture require the deconvolution of the individual peaks from the cumulative pattern by a systematic investigation. Although the area under each peak is directly proportional to the concentration of the component that the peak is arising from, the nonlinear absorption effects and unique microstructural features, such as the hollowness of the glass beads, complicate the analysis.

In order to accommodate these complications a series of standard samples with controlled concentrations were prepared for calibration. The diffraction patterns of the standard samples were analyzed to

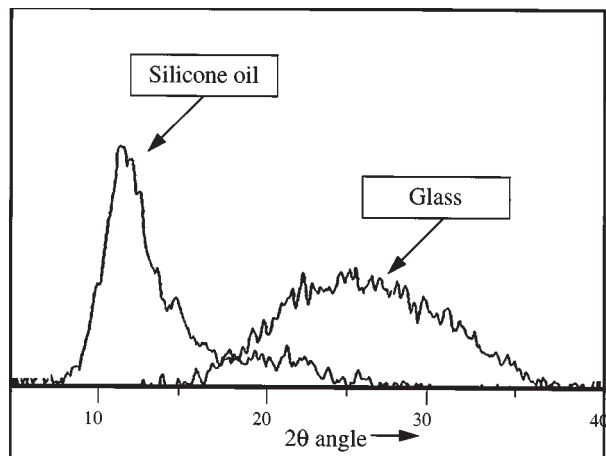


Fig. 5. Superimposed wide angle X-ray diffraction patterns of silicone 200 polymer and glass beads.

obtain a calibration curve for the volume fraction of the components (c_i) versus the integrated intensity fraction of the components. The calibration curve constructed by this method is shown in Fig. 6. Variations in concentration within ± 1 vol% around 60 vol% could be determined. A Rigaku DXR-3000 and a Siemens D-5000 computerized wide-angle diffractometers were used. The effective X-ray probe size used in degree of mixing analysis was 1 mm^2 . Various mixing indices were determined from these measurements using the statistical analysis discussed next.

Characterization of the Mixing Indices

Each sample was characterized upon N measurements of concentration c_i of the glass filler. The mean concentration was then calculated as:

$$\bar{c} = \frac{1}{N} \sum_{i=1}^N c_i \quad (21)$$

where the mean of the population, \bar{c} , should not differ significantly from the overall concentration of the glass filler, ϕ . The difference between \bar{c} and ϕ decreases as the number of the samples, N , increases. A basic measure of the homogeneity of a mixture is the extent to which the concentration values at various regions of the volume of the mixture differ from the mean concentration. The variance s^2 , arising from the individual concentration c_i measurements, provides such an index to quantitatively assess the degree of mixing. The variance is given by:

$$s^2 = \frac{1}{(N-1)} \sum_{i=1}^N (c_i - \bar{c})^2 \quad (22)$$

A small variance implies that most of the samples yield concentration c_i values which are close to the

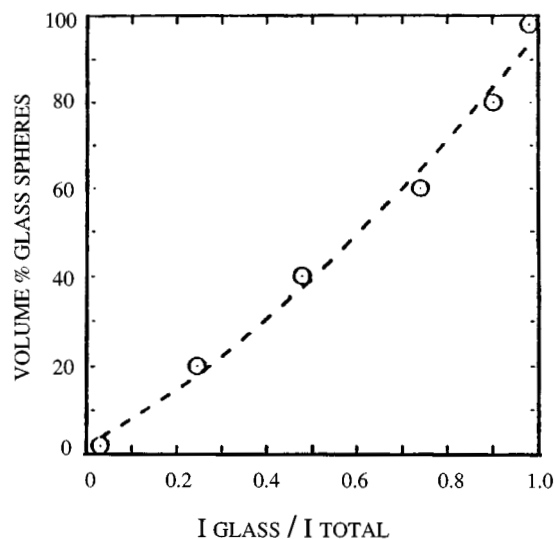


Fig. 6. Calibration curve for volume fraction of glass spheres in suspension versus WAXD integrated-intensity fraction of glass spheres in suspension.

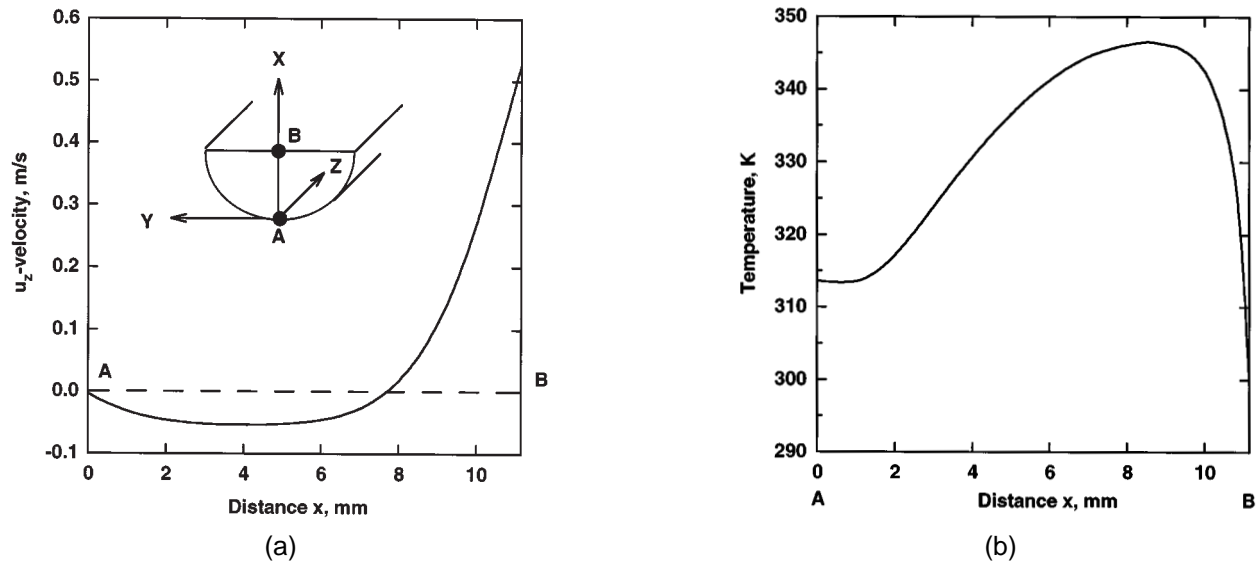


Fig. 7. Typical z -velocity and temperature distributions in the fully flighted section of the extruder for 210 rpm and 120 kg/hr at $z = 0.84$ m.

mean \bar{c} of all samples, suggesting the approach to a homogeneous system. A measure of the relative variability is defined with the coefficient of variation, v , which is the ratio of standard deviation to mean:

$$v = \frac{s}{\bar{c}} \quad (23)$$

The maximum variance occurs if the components are completely segregated. Maximum variance is given by:

$$s_0^2 = \bar{c}(1 - \bar{c}) \quad (24)$$

If the variance is normalized to its maximum value, the resulting parameter is called the intensity of segregation, I_{seg} (63, 64). This is given by:

$$I_{seg} = \frac{s^2}{s_0^2} = \frac{s^2}{\bar{c}(1 - \bar{c})} \quad (25)$$

A distributive mixing index, MI, can be defined as (61):

$$MI = 1 - \frac{s}{s_0} \quad (26)$$

For ideally homogeneous systems the intensity of segregation values approach zero and the mixing index values approach one.

RESULTS AND DISCUSSION

The typical downchannel velocity u_z , and temperature distributions at a screw rpm of 210 and a mass flow rate (120 kg/hr) are presented in Fig. 7 for a downchannel location $z = 0.84$ m. This flow rate is sufficiently high for the SUPG technique to successfully attenuate any instability in the temperature solution. In the velocity distribution a back flow region is located close to the screw root. Both the size and strength of this back flow region can change as a

result of the changes in shear viscosity of the suspension induced by temperature effects. In the corresponding temperature distribution, the occurrence of a high velocity gradient adjacent to the barrel surface generates significant viscous energy dissipation effects leading to a temperature hot spot adjacent to the barrel and a reversal of the direction of heat flux, i.e., from the bulk of the fluid to the barrel.

For the same case, the developments of the bulk temperature and the pressure gradient in the downchannel direction are shown in Fig. 8. As we proceed downchannel, the model predicts, as expected, a decrease in the pressure gradient. Even though the value of c' (0.00395 K^{-1}) of this suspension appears relatively low, the temperature increase over the selected downchannel distance is substantially high (approximately 35K). This produces a significant decrease in the pressure gradient. This effect becomes more pronounced as the screw rpm increases.

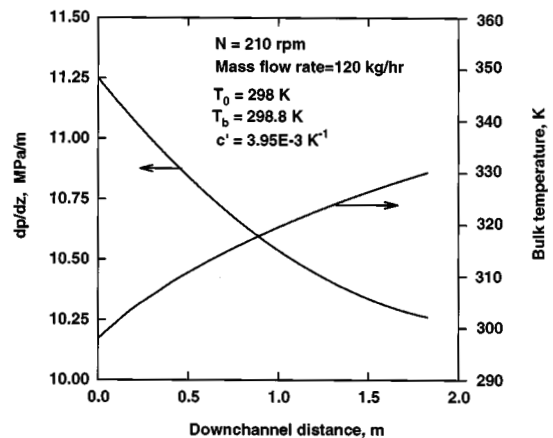


Fig. 8. Pressure gradient and bulk temperature development at 210 rpm and 120 kg/hr mass flow rate.

For the relatively low volume flow rates used in the experiments, the SUPG technique is no longer adequate, and the extrapolation procedure outlined earlier was implemented. In Figs. 9–12, the typical experimental pressure distributions are compared with the numerically predicted results for various values of screw rpm. The excellent agreement, most especially in the low to medium screw rpm range, suggests that when the wall slip behavior of the fluid and its shear viscosity are adequately characterized for a well-mixed and deaerated filled polymer the numerical predictions are reliable. The largest difference between the experimental and theoretical results was observed at the highest screw speed of 210 rpm where the viscous dissipation effect is large. An underestimation of the axially averaged bulk temperature used in estimating the shear viscosity could account for the observed dif-

ference. At this high screw rpm, were the SUPG technique to be adequate, the reduction of the shear viscosity with viscous energy dissipation would have given rise to a further decrease of the local pressure gradient. This would have resulted in a better agreement between the experimental and simulation results towards the end of the screw channel.

Figure 13 indicates that ignoring wall slip generates numerical predictions which would be significantly in error. This study therefore demonstrates that, for the numerical analysis to predict reliable results, wall slip behavior (if present) must be properly accounted for. Finally, in Fig. 14, we compare the experimentally obtained bulk temperatures with the numerically computed values. The agreement is acceptable and the differences ($\pm 5\%$) are within the experimental accuracy range.

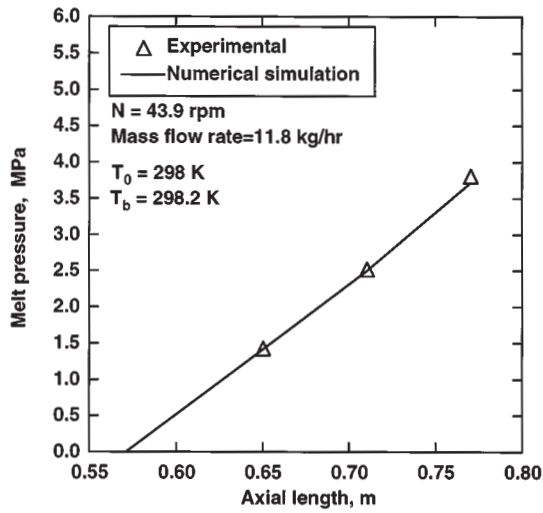


Fig. 9. Comparison of experimental and predicted pressure values at 44 rpm and 11.8 kg/hr.

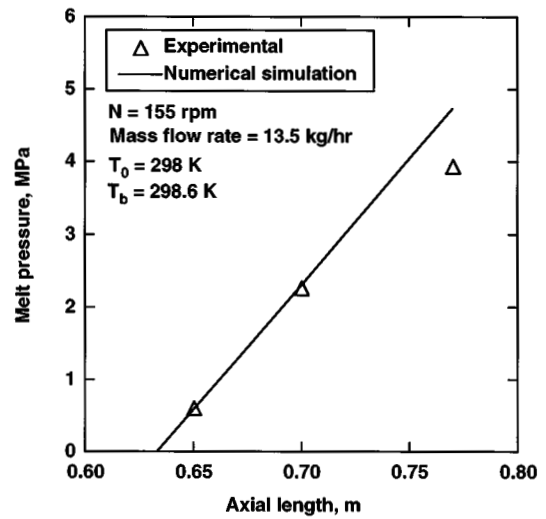


Fig. 11. Comparison of experimental and predicted pressure values at 155 rpm and 13.5 kg/hr.

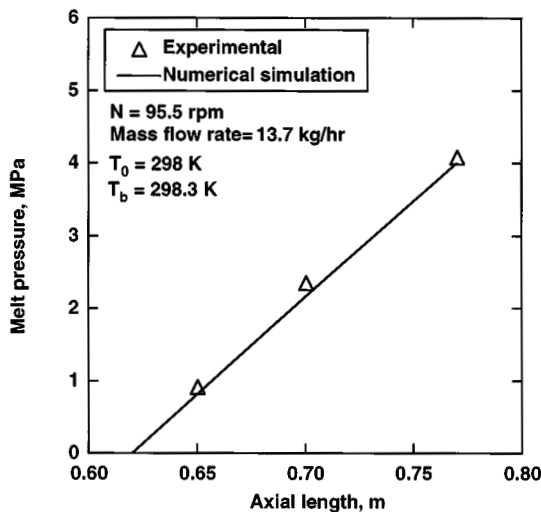


Fig. 10. Comparison of experimental and predicted pressure values at 95.5 rpm and 13.7 kg/hr.

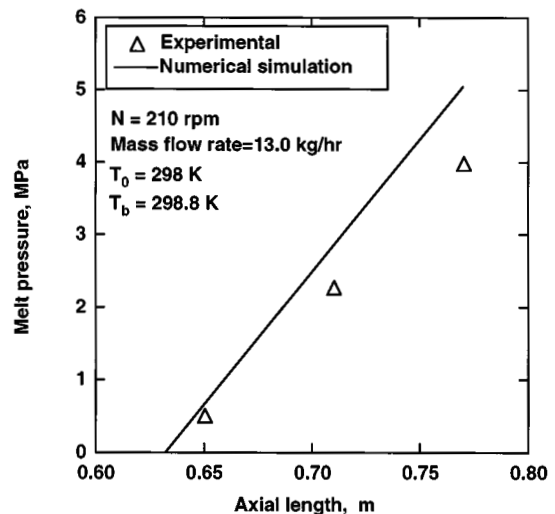


Fig. 12. Comparison of experimental and predicted pressure values at 210 rpm and 13.0 kg/hr.

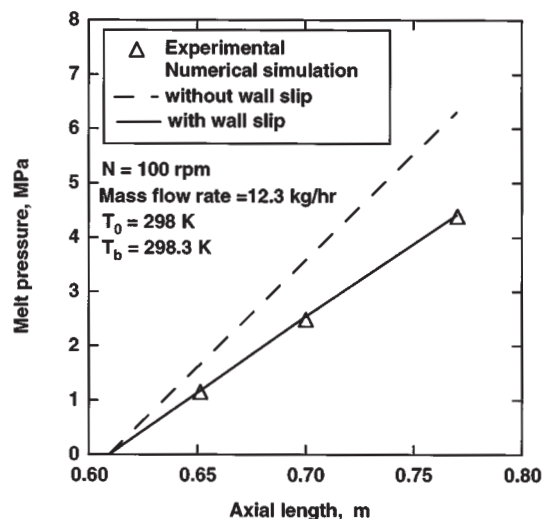


Fig. 13. Comparison of experimental and predicted pressure at 100 rpm and 12.3 kg/hr with and without the inclusion of wall slip in the simulation.

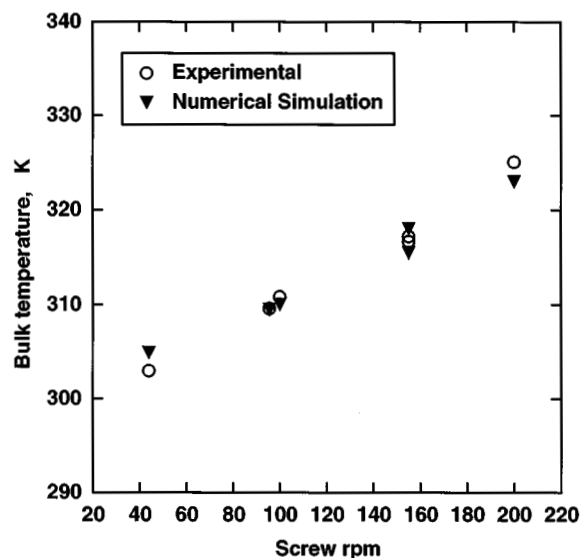


Fig. 14. Comparison of experimental and predicted bulk temperatures at various screw rotational speeds.

It should be noted that the heat transfer and pressurization results presented are provided for a polymer melt filled with solid particles when its air content is carefully removed. One can assume that the filler and the polymer are “sufficiently well mixed” in this section. The first question we have to address is whether that assumption is true and indeed what the state of the degree of mixing is. Since the rheological characterization of the filled polymer was carried out using samples that were collected upon extrusion, as well as using the on-line rheometer, i.e., the adjustable gap rheometer of the extruder, it is expected that the rheological behavior of the fluid is well known in this section of the extruder.

Degree of Mixing

The results of the state of mixing analysis of the twin-screw extruded samples are summarized in Table 1. The mean values of the volume percent of the glass were within 1% of the targeted values for the twin-screw extrusion (TSE) runs. The standard deviation and the 95% confidence intervals were negligible around the mean for the samples collected upon twin-screw extrusion, suggesting excellent mixing. To elucidate this further a batch mixed sample was also in-

cluded in the analysis. A Haake torque rheometer with a mini-Banbury mixing head was used for this experiment. The superiority of the state of distributive mixing in the twin-screw mixed samples is revealed by the lower coefficient of variation and intensity of segregation values and the higher mixing index values observed in these materials compared to those of the batch mixed sample. Thus, overall our WAXD technique assured us that the intended volume concentration of solids could indeed be incorporated into the polymer with twin-screw extrusion and that the samples analyzed were well-mixed.

Shortcomings

As indicated the analysis presented here was applied only to the regular flighted screw section of the extruder preceding the die where the suspension is well mixed as demonstrated above and properly de-aerated. However, the other screw sections (zones A-F in Fig. 2) present a number of additional challenges including:

1. The polymer and the filler are spatially differently distributed at each cross-section of the extruder, especially in the kneading disc based mixing section of the extruder. The amount of specific

Table 1. The Results of the WAXD Analysis of Mean Solid Concentrations and Degree of Mixing Parameters of the Batch Mixed and Twin-Screw Extruded Suspensions of Silicone Oil With Targeted 60 vol% Glass Beads.

	Mean %	Standard Deviation	Coeff. of Variation	Mixing Index	Intensity of Segregation	95% Confid. Interval
Batch Mixed	60.0	1.40	0.023	0.97148	8.1E-04	3.464
1st TSE Run	60.6	0.35	0.006	0.99995	5.0E-05	0.859
2nd TSE Run	60.9	0.22	0.004	0.99998	2.0E-05	0.344
1st and 2nd TSE Runs	60.8	0.30	0.005	0.99996	3.7E-05	0.276
Beginning	60.8	0.07	0.001	1.00000	2.1E-06	0.602
End	61.1	0.21	0.003	0.99998	1.9E-05	1.805

energy input incorporated into the material increases in the downchannel direction with concomitant changes in the spatial distributions of the ingredients and the rheological behavior of the suspension.

- The air content generates a third phase, which is again continuously altered in its volume content and distribution in the downchannel direction in the mixing section prior to devolatilization in the subsequent section of the extruder.

The typical change in the rheological behavior of a filled polymer with increasing specific energy input is shown in Fig. 15. The shear viscosity of an acrylonitrile terminated polybutadiene polymer filled with 60 vol% ammonium sulfate was found to decrease with increasing specific energy input in a torque rheometer (65). Kalyon *et al.* (9) have shown that the specific energy input in the extruder, E_s , can be calculated as a function of position as:

$$U_x \frac{E_s}{\partial x} + U_y \frac{\partial E_s}{\partial y} + U_z \frac{\partial E_s}{\partial z} = \left(\frac{1}{\rho} \right) |\dot{\gamma}| |\tau| \quad (27)$$

where $|\dot{\gamma}|$ and $|\tau|$ are the second invariants of the rate of deformation and the stress tensors, respectively. The specific energy input E_s , is used in the calculation of the viscosity at each point of the flow domain. The calculation and use of the specific energy input in simulation was shown to make a large difference for twin-screw extrusion of filled polymers (9).

The rheology and extrudability of the filled polymer are also significantly affected by the presence and distribution of air. Kalyon and co-workers have shown that the presence of air in the suspension, especially at the partially filled sections of the processor where free surfaces exist, gives rise to a decrease in the shear viscosity of the suspension and to an increase in its

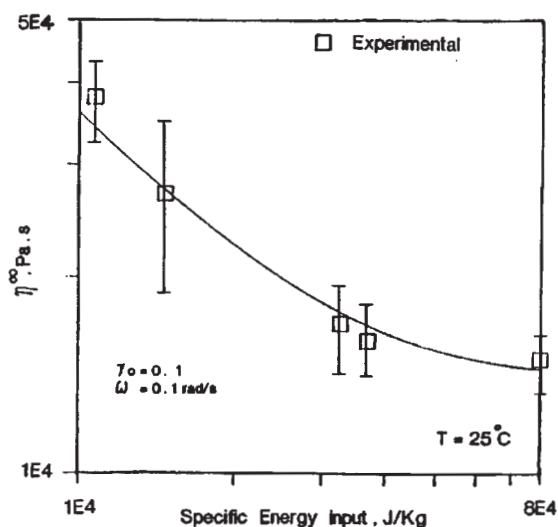


Fig. 15. The ratio of the amplitude of the shear stress over the amplitude of the strain in large amplitude shear flow vs specific energy input for 60 vol% ammonium sulfate in acrylonitrile terminated polybutadiene binder polymer (65).

Navier's wall slip coefficient (37). However, the determination of air content along the extruder and the concomitant changes in rheological behavior have not been attempted here. Clearly, these two areas, i.e., the changing microstructure and air content and the resulting changes in rheological behavior are significant factors in extrusion of filled polymers and need to be incorporated if the rest of the twin-screw extruder (i.e., feeding, mixing and devolatilization sections) are to be mathematically modeled. No attempt was made here to tackle this problem.

CONCLUSIONS

A combined experimental and finite element approach has been successfully implemented in the study of flow and heat transfer in twin-screw extrusion of concentrated suspensions. The numerical method accounts for both the viscoplastic and wall slip behavior encountered with concentrated suspensions. Furthermore, a numerical calculation procedure for obtaining bulk temperature distributions in extrusion flows for low volume (or mass) flow rates with significant back-flow, for which the SUPG method fails, has been outlined and implemented.

To our knowledge this is the first time that experimental twin-screw extrusion data for a concentrated suspension that exhibits viscoplasticity and wall slip were compared with the results of numerical simulation. The results of this study underscore the need to incorporate the proper interfacial flow boundary condition at the wall (i.e., wall slip) for fluids such as concentrated suspensions, gels, etc., which exhibit wall slip behavior. A wide angle X-ray analysis based technique was also demonstrated and used to determine quantitatively the degree of distributive mixing of the filler in the polymer upon the mixing occurring in the twin-screw extruder. The direct determination of the spatial distribution of the filler particles and the resulting quantitative measures of the degree of mixing should provide the wherewithal necessary to link the ultimate properties of a filled material to its state of mixedness achieved upon extrusion.

ACKNOWLEDGMENTS

The project has been supported by BMDO/IST as managed by Dr. Richard S. Miller and Dr. Judah Goldwasser of Naval Research under contract number N00014-95-1-0770 and through the partial support of IFPRI.

NOMENCLATURE

c'	temperature coefficient of viscosity
C_p	specific heat capacity
dp_m/dz	mean viscous pressure gradient
dp_m^*/dz^*	dimensionless mean viscous pressure gradient
G	Griffith number = $m_0 \omega^{n-1} (\omega R_s)^2 / k (T_p - T_0)$
\mathbf{i}	unit vector in the x -coordinate direction
\mathbf{k}	unit vector in the z -coordinate direction

k	thermal conductivity	ϕ	loading level of suspension
ℓ	axial coordinate direction	ϕ_h	helix angle of the screw element
m_o	material parameter	π	weighting function for the momentum equations
n	parameter governing the sensitivity of fluid to deformation rate	θ	dimensionless temperature $= (T - T_0)/(T_b - T_0)$
\mathbf{n}	unit outward normal vector	θ_b	dimensionless bulk temperature
n_b	stress growth exponent	θ'	Bragg angle
n_b^*	dimensionless stress growth exponent	ρ	density
\bar{p}	transverse pressure	ρ_c	ratio of centerline distance to screw radius
\bar{p}^*	dimensionless transverse pressure, $\bar{p}/(m_o\omega^n)$	σ	upwinding parameter
p_m	mean viscous pressure	τ_{12}	shear stress in 12 direction
p_m^*	dimensionless mean viscous pressure, $p_m/(m_o\omega^n)$	τ_y	apparent yield stress
Pe	Péclet number $= \rho C_p \omega R_s^2/k$	τ_y^*	dimensionless apparent yield stress
Q	volume flow rate	$\underline{\tau}$	deviatoric stress tensor
Q^*	dimensionless volume flow rate	ω	screw rotational speed
R_s	screw radius		
\mathbf{t}	unit tangent vector		
T	temperature		
T_b	barrel temperature		
T_0	entrance temperature		
\mathbf{T}	total stress tensor		
u_x	velocity component in the x -coordinate direction		
u_y	velocity component in the y -coordinate direction		
u_z	velocity component in the z -coordinate direction		
U_x^*	dimensionless velocity component in the x -coordinate direction, $u_x/(\omega R_s)$		
U_y^*	dimensionless velocity component in the y -coordinate direction, $u_y/(\omega R_s)$		
U_z^*	dimensionless velocity component in the z -coordinate direction, $u_z/(\omega R_s)$		
\mathbf{u}	velocity vector		
\mathbf{u}^*	dimensionless velocity vector		
$\mathbf{u}^{\text{solid}}$	boundary velocity vector		
ω^f	discontinuous perturbation function on W^f		
W^f	continuous weighting function		
\bar{W}^f	weighting function for the energy equation		
x	x -coordinate direction		
x^*	dimensionless x -coordinate direction, x/R_s		
\mathbf{x}	vector of nodal unknowns		
y	y -coordinate direction		
y^*	dimensionless y -coordinate direction, y/R_s		
z	helical z -coordinate direction		
z^*	dimensionless z -coordinate direction, z/R_s		
β^*	dimensionless Navier's slip coefficient		
$\dot{\gamma}$	deformation rate		
$ \dot{\gamma} $	magnitude of the rate-of-deformation tensor defined in Eq 13		
$ \dot{\gamma} ^*$	dimensionless magnitude of the rate-of-deformation tensor		
$\underline{\dot{\gamma}}$	rate-of-deformation tensor		
η	shear viscosity material function		
η^*	dimensionless shear viscosity material function		
λ_s	penalty parameter for the kinematic condition		

REFERENCES

1. C. Rauwendaal, *Polymer Extrusion*, Hanser Verlag, Munich (1986).
2. J. L. White, *Twin Screw Extrusion*, Hanser Verlag, Munich (1990).
3. D. M. Kalyon, "Applications of Continuous Mixers," *Encyclopedia of Engineering Materials*, N. Cheremisinoff, ed., Marcel Dekker, New York (1988).
4. M. L. Booy, *Polym. Eng. Sci.*, **18**, 973 (1978).
5. C. D. Denson and B. K. Hwang, *Polym. Eng. Sci.*, **20**, 965 (1980).
6. M. L. Booy, *Polym. Eng. Sci.*, **20**, 1220 (1980).
7. J. L. White, W. Szydlowski, K. Min, and M. Kim, *Adv. Polym. Techn.*, **7**, 295 (1987).
8. D. M. Kalyon, A. D. Gotsis, C. G. Gogos, and C. Tsenoglou, *SPE ANTEC Technical Papers*, **34**, 64 (1988).
9. D. M. Kalyon, A. Gotsis, U. Yilmazer, C. Gogos, H. Sangani, B. Aral, and C. Tsenoglou, *Advances in Polymer Technology*, **8**, 337 (1988).
10. Y. Wang, J. L. White, and W. Szydlowski, *Intern. Polym. Processing*, **4**, 262 (1989).
11. Y. Wang and J. L. White, *J. Non-Newt. Fluid Mech.*, **32**, 19 (1989).
12. W. Szydlowski and J. L. White, *Int. Polym. Proc.*, **3/4**, 142 (1988).
13. R. A. Lai-Fook, A. Senouci, and A. C. Smith, *Polym. Eng. Sci.*, **29**, 433 (1989).
14. A. D. Gotsis, Z. Ji, and D. M. Kalyon, *SPE ANTEC Technical Papers*, **36**, 139 (1990).
15. Z. Ji and D. M. Kalyon, *SPE ANTEC Technical Papers*, **38**, 1323 (1992).
16. A. Lawal, D. M. Kalyon, and Z. Ji, *Polym. Eng. Sci.*, **33**, 140 (1993).
17. A. Lawal and D. M. Kalyon, *SPE ANTEC Technical Papers*, **39**, 3397 (1993).
18. A. Lawal and D. M. Kalyon, *Polym. Eng. Sci.*, **35**, 1325 (1995).
19. A. Lawal and D. M. Kalyon, *J. Applied Polymer Science*, **58**, 1501 (1995).
20. H. Yang and I. Manas-Zloczower, *Polym. Eng. Sci.*, **32**, 1411 (1992).
21. H. Meijer and P. Elemans, *Polym. Eng. Sci.*, **28**, 275 (1988).
22. H. Cheng and I. Manas-Zloczower, *Polym. Eng. Sci.*, **37**, 1082 (1997).
23. H. G. Karian, *J. Vinyl Tech.*, **7**, 154 (1985).
24. D. M. Kalyon, R. Yazici, C. Jacob, B. Aral, and S. W. Sinton, *Polym. Eng. Sci.*, **31**, 1386 (1991).
25. D. B. Todd, *Polym. Eng. Sci.*, **15**, 437 (1975).
26. C. J. Rauwendaal, *Polym. Eng. Sci.*, **21**, 1092 (1981).
27. D. Bigio and L. Erwin, *SPE ANTEC Technical Papers*,

- 31**, 45 (1985).
28. D. M. Kalyon and H. N. Sangani, *SPE ANTEC Technical Papers*, **35**, 124 (1989).
 29. D. M. Kalyon and H. Sangani, *Polym. Eng. Sci.*, **29**, 1018 (1989).
 30. D. M. Kalyon, A. Gotsis, C. Gogos, and C. Tsenoglou, *Innovative Science and Technology Symposium of SPIE, Propulsion*, 71 (1988).
 31. D. M. Kalyon, C. Jacob, and P. Yaras, *Plastics, Rubber and Composites Processing and Applications*, **16**, 193 (1991).
 32. M. Essseghir, PhD thesis, Rutgers University, New Jersey (1991).
 33. R. B. Bird, G. C. Dai, and B. J. Yarusso, *Rev. in Chem. Eng.*, **1**, 1 (1983).
 34. U. Yilmazer and D. M. Kalyon, *J. Rheol.*, **33**, 1197 (1989).
 35. D. M. Kalyon, P. Yaras, B. Aral, and U. Yilmazer, *J. Rheol.*, **37**, 35 (1993).
 36. B. Aral and D. M. Kalyon, *J. Rheol.*, **38**, 957 (1994).
 37. B. Aral and D. M. Kalyon, *Plast. and Rubber Comp. Proc. and Applications*, **24**, 201 (1995).
 38. B. Aral and D. M. Kalyon, *J. Rheol.*, **41**, 599 (1997).
 39. H. E. H. Meijer and C. P. J. M. Verbraak, *Polym. Eng. Sci.*, **28**, 758 (1988).
 40. Z. Ji, A. Gotsis, and D. M. Kalyon, *SPE ANTEC Technical Papers*, **36**, 160 (1990).
 41. A. Lawal and D. M. Kalyon, Proceedings of the First International Conference on Transport Phenomena in Processing, 985, S. Guceri, ed., Technomic Publ. Co., (1992).
 42. A. Lawal and D. M. Kalyon, *SPE ANTEC Technical Papers*, **39**, 2782 (1993).
 43. A. Lawal, D. M. Kalyon, and U. Yilmazer, *Chem. Eng. Comm.*, **122**, 127 (1993).
 44. A. Lawal and D. M. Kalyon, *Numerical Heat Transfer*, **26**, 103 (1994).
 45. A. Lawal and D. M. Kalyon, *Polym. Eng. Sci.*, **34**, 1471 (1994).
 46. A. Lawal and D. M. Kalyon, *Chem. Eng. Sci.*, **52**, 1323 (1996).
 47. A. Lawal, S. Railkar, P. Yaras, and D. M. Kalyon, *J. Materials Processing and Manufacturing Science*, **5**, 57 (1996).
 48. W. T. Silliman and L. E. Scriven, *J. Comp. Phys.*, **34**, 287 (1980).
 49. J. Zi, A. D. Gotsis, and D. M. Kalyon, *SPE ANTEC Technical Papers*, **36**, 160 (1990).
 50. T. C. Papanastasiou, *J. Rheol.*, **31**, 385 (1987).
 51. T. J. R. Hughes and A. N. Brooks, "A Multi-Dimensional Upwind Scheme with No Crosswind Diffusion," in T. J. R. Hughes, ed., *Finite Element Methods for Convection Dominated Flows*, Vol. 34, p. 19, ASME, New York (1979).
 52. A. B. Brooks and T. J. Hughes, *Comput. Methods App. Mech. Eng.*, **32**, 199 (1982).
 53. C. C. Yu and J. C. Heinrich, *Int. J. Numer. Methods Eng.*, **24**, 2201 (1987).
 54. T. J. R. Hughes, M. Mallet, and A. Mizukami, *Comput. Methods Appl. Mech. Eng.*, **54**, 341 (1986).
 55. A. Lawal, S. Railkar, and D. M. Kalyon, *Intern. Polym. Processing*, **12**, 123 (1997).
 56. J. R. Pearson, *Mechanics of Polymer Processing*, Chap. 11, Elsevier Applied Science Publishers, London (1985).
 57. D. M. Kalyon and H. Gokturk, "Adjustable Gap Rheometer," U.S. Patent 5,277,058 (1994).
 58. P. Yaras, PhD thesis, Stevens Institute of Technology, New Jersey (1996).
 59. R. Yazici and D. M. Kalyon, *Rubber Chem. Technol.*, **66**, 527 (1993).
 60. R. Yazici and D. M. Kalyon, *SPE ANTEC Technical Papers*, **39**, 2845 (1993).
 61. R. Yazici and D. M. Kalyon, *J. Energetic Materials*, **14**, 57 (1996).
 62. R. Yazici and D. M. Kalyon, *SPE ANTEC Technical Papers*, **43**, 2076 (1997).
 63. D. M. Kalyon, in *Encyclopedia of Fluid Mechanics*, Vol. 7, Ch. 28, 887-926, N. Cheremisinoff, ed. Gulf Publishing, Houston (1988).
 64. W. D. Mohr, *Processing of Thermoplastic Materials*, E. Bernhard, ed., Krieger Publishing Co., Malabar (1959).
 65. B. Aral, M.Eng. thesis, Stevens Institute of Technology, New Jersey (1990).